Chinese Chemical Letters 36 (2025) 110007

Contents lists available at ScienceDirect

Chinese Chemical Letters

journal homepage: www.elsevier.com/locate/cclet

A 3D dual layer host with enhanced sodiophilicity as stable anode for high-energy sodium metal batteries

Run Chai[a], Qiujie Wu[a], Yongchao Liu[a], Xiaohui Song[a,b], Xuyong Feng[a,b], Yi Sun[a,b,*], Hongfa Xiang[a,b,*]

[a] Department of Materials Science and Engineering, Hefei University of Technology, Hefei 230009, China
[b] Engineering Research Center of High Performance Copper Alloy Materials and Processing, Ministry of Education, Hefei University of Technology, Hefei 230009, China

ARTICLE INFO

Article history:
Received 5 March 2024
Revised 15 April 2024
Accepted 13 May 2024
Available online 14 May 2024

Keywords:
3D current collector
Sodiophilicity
Low N/P ratio
Sodium metal batteries
Anode free

ABSTRACT

Sodium metal batteries (SMBs) have drawn much attention as complement to lithium metal batteries for next generation high-energy batteries. However, it is still a big challenge to enhance their cycling stability without sufficient sodium reserve in anode, due to the non-uniform Na plating/stripping and uncontrolled Na dendrite growth. Herein, a dual layer host consists of sodiophilic graphene@antimony nanoparticles bottom layer and 3D polyacrylonitrile nanofiber top layer (PAN-G@Sb) is employed to enable highly reversible Na plating/stripping. Thanks to the uniform Na deposition, PAN-G@Sb delivers an outstanding average Coulombic efficiency of 99.8%, highly reversible Na plating/stripping for 1000 cycles at 2.0 mA/cm^2, as well as over 1000 h of stable operation in symmetric cells. When paired with a high mass loading $Na_3V_2(PO_4)_3$ (NVP) cathode (16.2 mg/cm^2), the full cell (N/P ratio = 1.4) also displays prominent capacity retention of 98.7% after 250 cycles with a high energy density of 284.6 Wh/kg. Moreover, PAN-G@Sb||NVP anode-free full cell also shows an excellent capacity retention of 91.0% after 50 cycles at 0.5 C, exhibiting the stable operation of high energy SMBs.

Considering the limited geographical distribution of lithium and the increasing demand of large-scale battery applications [1,2], it is reasonable to develop sodium-ion batteries (SIBs) as alternatives to lithium-ion batteries due to the natural abundance of sodium (Na) resource and cost advantage [3-5]. Metallic Na has a low redox potential (−2.71 V *vs.* standard hydrogen) and a high theoretical special capacity (≈1166 mAh/g), indicating a great potential to establish high energy density battery system [6]. However, similar to lithium, the high reactivity of metallic Na brings severe interfacial parasitic reactions [7,8]. In particular, the uncontrolled dendrite growth is caused by uneven Na nucleation and deposition, leading to fast capacity fading and even safe issues [6,9-11].

To address above challenging issues, numerous strategies have been developed, such as optimizing electrolytes to *in-situ* form stable solid electrolyte interphase (SEI) [12-14], constructing artificial SEI layers to alleviate interfacial reactions [15,16], developing solid-state electrolytes to suppress dendrite growth [17,18], and engineering 3D current-collectors to accommodate volume change of Na metal anode [19-21]. Moreover, sodiophilic heterogeneous elements (such as Ag [22], Au [23], F [24], N [25]) have been recently introduced into current-collectors as heterogeneous crystal species to promote metal wettability and reduce the nucleation/growth overpotential. For example, Wu's team reported an inspiring strategy to achieve long-term stable and uniform deposition of Na metal through a nucleation buffer layer composed of carefully designed core-shell C@Sb nanoparticles [26].

However, these strategies usually are performed with thick Na anode (thicker than 100 μm) or high N/P ratio (area capacity ratio of negative to positive electrodes, usually higher than 15) in current researches [27-29], suggesting the demand of excess Na to compensate the consumption in parasitic reactions, such as continuous SEI reforming and "dead" (inactive) Na formation [30,31]. Unfortunately, thick metallic anode with excess Na not only reduce the high energy advantage of sodium metal batteries (SMBs), but also create the safety hazards due to its high chemical activity [30]. Thus, it is necessary to explore stable Na metal anode with limited Na for future high energy SMBs. The anode current-collectors play a critical role to influence the reversibility of metallic Na [32,33]. Since there is limited Na in low N/P SMBs or even anode-free SMBs, the capacity and lifespan of cell will be directly impacted by

* Corresponding authors.
E-mail addresses: suny@hfut.edu.cn (Y. Sun), hfxiang@hfut.edu.cn (H. Xiang).

https://doi.org/10.1016/j.cclet.2024.110007
1001-8417/

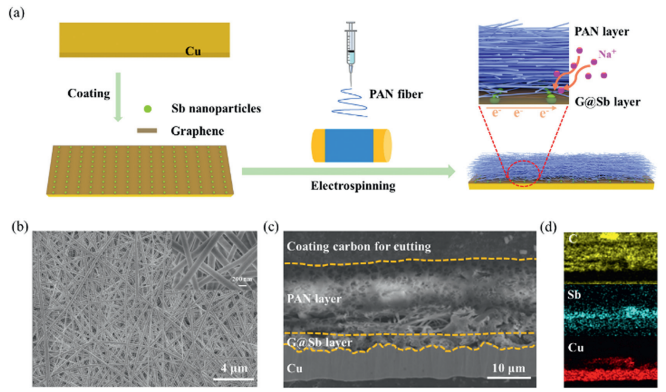

Fig. 1. (a) Schematic representation of the process of preparation of PAN-G@Sb. (b) SEM image of top of PAN-G@Sb. (c) SEM image of cross-section of PAN-G@Sb. (d) Corresponding EDS elements mapping of cross-section of PAN-G@Sb.

the initial Coulombic efficiency (ICE) and irreversible Na consumption, which are much more challenging to induce homogeneous Na deposition and impede dendrite growth. Therefore, reduction of Na nucleation barrier and regulation of subsequent Na plating/stripping are crucial to achieve suitable current-collectors for SMBs under limited Na condition. We have developed a dual layer structure with sodiophilic layer composed of graphene@antimony nanoparticles (G@Sb) and 3D protective layer constructed of polyacrylonitrile (PAN) nanofibers (PAN-G@Sb) to spatially control Na deposition. The G@Sb layer offers abundant nucleation sites to guide the homogeneous Na plating, due to its high Na affinity. The PAN layer confine Na deposition to suppress dendrite growth, ascribed to its insulating 3D framework. As a result, the dual layer host display an impressive average Coulombic efficiency of 99.8%, stable Na plating/stripping for 1000 cycles at a current density of 2.0 mA/cm^2 with 1.0 mAh/cm^2 capacity, and over 1000 h of stable operation in symmetric cells at 2.0 mA/cm^2. The full cell (N/P ratio = 1.4) using thick NVP cathode (16.2 mg/cm^2) and Na-PAN-G@Sb host (2 mAh/cm^2 Na pre-deposition) exhibits high cycling stability with capacity retention of 98.7% after 250 cycles and reaches an excellent energy density over 280 Wh/kg. Moreover, the anode-free full cell also displays a superior capacity retention of 91.0% at 0.5 C after 50 cycles, demonstrating the stable operation of high energy SMBs.

As illustrated in Fig. 1a, the 3D dual layer host is fabricated by coating G@Sb on Cu foil combined with subsequent electrospinning technology. Fig. 1b illustrates the 3D network structure at the top of the PAN fiber. As shown in Figs. 1c and d, the thickness of G@Sb bottom layer and PAN framework top layer is around 4 μm and 18 μm, respectively (The carbon layer on PAN layer is coated for Ar ion beam cutting). The ball milled Sb nanoparticles with 53.1% mass ratio are uniformly distributed within graphene sheets (Figs. S1a, b and S2 in Supporting information), which is confirmed by energy dispersive spectroscopy (EDS) mapping and X-ray diffraction (XRD) pattern (Figs. S1c and S3 in Supporting information). The 3D framework is interwoven by PAN fibers with uniform diameter of 200 nm. The chemical composition of PAN was analyzed by X-ray photoelectron spectroscopy (XPS) measurements (Fig. S4 in Supporting information). The characteristic peaks of O, N, and C are displayed in XPS full spectrum (Fig. S4a). The fitted peaks of N 1s spectrum represent the existence of pyrrolic-N (400.6 eV), and pyridinic-N (398.2 eV), while O 1s spectrum can be divided into three peaks corresponding to C=O bond (530.3 eV), O–H bond (530.8 eV), and C–O bond (531.9 eV) (Figs. S4b and c in Supporting information). The abundant sodiophilic N and O play a critical role in spatially regulating Na^+ distribution, thus enhancing the uniform deposition of Na [19,34,35].

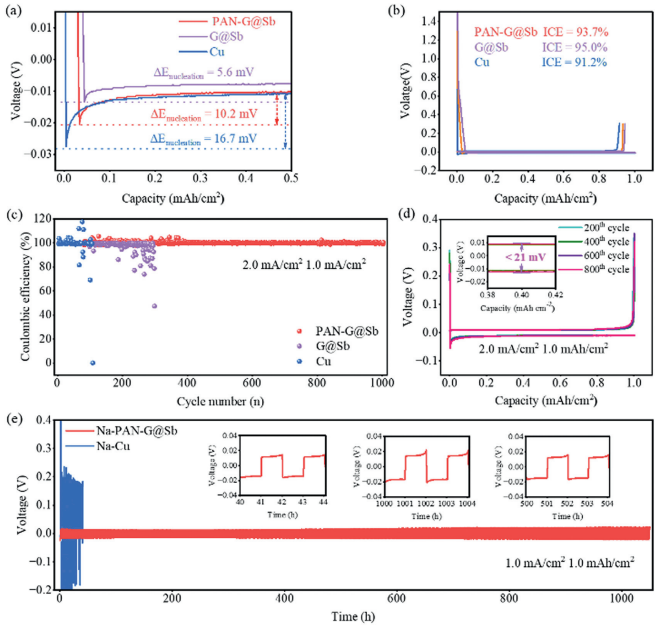

Fig. 2. (a) Nucleation overpotential profile of Na plating for PAN-G@Sb, G@Sb, Cu at 1.0 mA/cm^2. (b) ICE of PAN-G@Sb, G@Sb, Cu at 1.0 mA/cm^2 with 1.0 mAh/cm^2. (c) CE of Na plating/stripping on PAN-G@Sb, G@Sb, Cu at 2.0 mA/cm^2 with 1.0 mAh/cm^2 and (d) corresponding galvanostatic discharge/charge profiles. (e) Voltage profiles of symmetric cells with Na-Cu and Na-PAN-G@Sb electrodes at 1.0 mA/cm^2 with 1.0 mAh/cm^2.

The half cells (Cu||Na, G@Sb||Na and PAN-G@Sb||Na) with 1 mol/L $NaPF_6$ in dimethoxyethane (DME) as electrolyte are assembled to evaluate the Na plating/stripping performance of different substrates. As shown in Fig. 2a, compared to the initial nucleation overpotential for bare Cu foil (16.7 mV), it significantly declined after introduction of G@Sb layer, which suggests that the sodiophilic Sb nanoparticles reduce the nucleation barrier of Na deposition and disperse the Na ions flux. Fig. 2b exhibits initial voltage profiles of Na plating-stripping process for the cells with the capacity of 1.0 mAh/cm^2. The substrates with G@Sb layer show an alloy plateau ($3Na + Sb = Na_3Sb$) at the beginning of the discharge, which facilitates the uniform SEI formation, leading to rising ICE of 95.0% and 93.7% for G@Sb||Na and PAN-G@Sb||Na, respectively. The cut-off voltage of cells is fixed at 0.3 V to maintain the stabilization of Na_3Sb (Fig. S5 in Supporting information). The larger contact area between the electrolyte and 3D framework leads to the relative lower ICE for PAN-G@Sb||Na. The rate performance of the cells was tested using different current densities from 0.5 mA/cm^2 to 4.0 mA/cm^2 (Fig. S6a in Supporting information). Both PAN-G@Sb||Na and G@Sb||Na exhibit high cycling stability with nearly same overpotential (36.2 mV, 36.8 mV) at 4.0 mA/cm^2, much lower than Cu||Na (67.6 mV) (Fig. S6b in Supporting information). Fig. 2c displays the CE of Na plating/stripping for PAN-G@Sb||Na maintains above 99% after 1000 cycles at 2.0 mA/cm^2. In comparison, the CE of Cu||Na appears severe fluctuation after 50 cycles, as well as the G@Sb||Na after 250 cycles, indicating the 3D PAN framework can effectively suppress Na dendrite growth in long term cycle. The corresponding voltage profiles of PAN-G@Sb||Na at different cycles are obviously overlapped with the low voltage hysteresis of less than 21 mV even after 800 cycles (Fig. 2d and Fig. S7 in Supporting information). In order to achieve accurate Na plating/stripping efficiency on plated Na substrate, Aurbach CE tests are also employed [36]. A single Na plating/stripping cycle at 10.0 mAh/cm^2 was performed on bare Cu foil and PAN-G@Sb to eliminate the ICE influence of different substrates. Then 10.0 mAh/cm^2 of Na was pre-deposited on PAN-G@Sb and Cu as a

Na reservoir (Q_T). After that, the cells were cycled 10 times with a fixed capacity of 1.0 mAh/cm^2 (Q_C) at 1.0 mA/cm^2 and stripped to 0.3 V in the end (Q_S). The average Coulombic efficiency was calculated by Eq. 1.

$$CE_{avg} = (nQ_C + Q_S)/(nQ_C + Q_T) \quad (1)$$

The Na average CE of Cu foil is only 86.0%, much lower than that of 99.8% on PAN-G@Sb (Fig. S8 in Supporting information). As the areal capacity are increased from 1.0 mAh/cm^2 to 10.0 mAh/cm^2, the PAN-G@Sb||Na still demonstrates a highly reversible Na plating/stripping process (Fig. S9 in Supporting information).

The symmetric cells were assembled to evaluate the interfacial stability of bare Cu foil and PAN-G@Sb. As shown in Fig. 2e, the cell using PAN-G@Sb shows a stable cycling over 1000 h at 1.0 mA/cm^2 with 1.0 mAh/cm^2 and displays a low voltage hysteresis in the range of 14.5–22.0 mV. When the current increased to 2.0 mA/cm^2, the cell still maintains the cycling stability over 1000 h (Fig. S10a in Supporting information). In contrast, the cells with bare Cu foil exhibit unstable and irregular voltage hysteresis at a current density of both 1.0 mA/cm^2 and 2.0 mA/cm^2, which are short-circuited after 11 and 9 h, respectively. The rate performance of the symmetric cells at different current densities with a fixed areal capacity 1.0 mAh/cm^2 are estimated (Fig. S10b in Supporting information). The G@Sb sodiophilic layer and 3D PAN framework enables the cell with an available current density up to 8.0 mA/cm^2, indicating the highly rate capability of PAN-G@Sb.

The morphologies of Na plating/stripping on different substrates after 10 cycles are characterized by SEM analysis. An irregular cracked surface can be observed on bare Cu foil at 1.0 mA/cm^2 with 2.0 mAh/cm^2 depositions (Fig. 3a), which becomes mossy after Na stripping off (Fig. 3e), indicating the residual "dead Na". In comparison, with the introduction of G@Sb layer, there is a dense and uniform Na deposition layer on the surface, which displays highly reversible as well (Figs. 3b and f). For PAN-G@Sb substrate (Figs. 3c, d, g and h), most of Na deposits on the bottom of G@Sb layer when the capacity is 2.0 mAh/cm^2, which is consistent with EDS mapping of Na distribution (Figs. 3i-m). With the capacity increased to 6.0 mAh/cm^2, a large amount of Na deposits into the 3D PAN framework without dendrite formation (Figs. 3d and h), demonstrating that the PAN-G@Sb enable a uniform and stable Na plating/stripping along the lateral plane of host, which should be due to the synergistic effects of uniform Na nucleation by sodiophilic G@Sb layer as well as homogeneous Na distribution by 3D PAN framework.

To investigate the feasibility of PAN-G@Sb substrate, limited amount of Na (2.0 mAh/cm^2) was pre-deposited on it to obtain the Na-PAN-G@Sb anode before full cells were assembled. The cells were based on these anodes and NVP cathode. In a SMBs by pairing excess Na metal anode, the NVP delivers a capacity of 108.6 mAh/g at 1 C (117.0 mA/g) (Fig. S11 in Supporting information). In order to verify the performance of PAN-G@Sb in high energy SMBs, the full cells were assembled with a low N/P ratio of 1.4 (Fig. 4a, loading mass of NVP up to 16.2 mg/cm^2), providing a high energy density of 284.6 Wh/kg at a rate of 0.33 C (based on total active material of cathode and anode, including pre-deposited Na), displaying a 98.7% capacity retention after 250 cycles (per cycle capacity decay rate of 0.005%). The corresponding voltage profiles of the cell at different cycle numbers are shown in Fig. 4b, suggesting the high cycling stability due to the nearly overlapped charge/discharge curves. In contrast, the full cell with same N/P ratio using Na-Cu anode exhibits rapidly capacity decay,

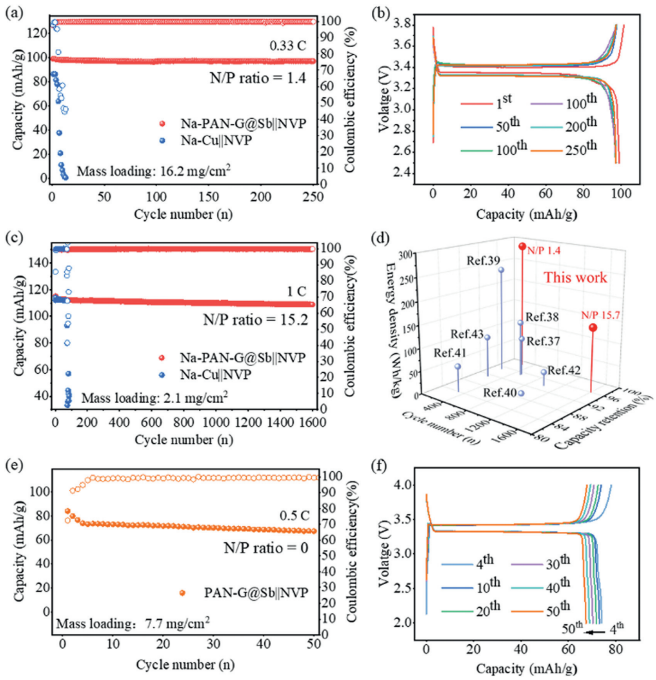

Fig. 4. (a) Cycling performance of the full cells at a rate of 0.33 C (N/P ratio = 1.44). (b) Corresponding charge/discharge profiles of Na-PAN-G@Sb||NVP from 1 to 250 cycles. (c) Cycling performance of the full cells at a rate of 1 C (N/P ratio = 15.7). (d) Ragone plot for the full cells compared to previously reported SMBs. (e) Cycling performance of the full cells at a rate of 0.5 C (N/P ratio = 0). (f) Corresponding charge/discharge profiles of PAN-G@Sb||NVP from 4 cycles to 50 cycles.

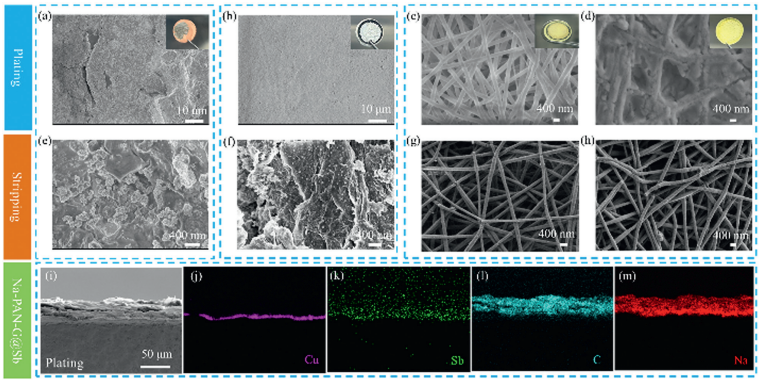

Fig. 3. SEM images of (a) Cu, (b) G@Sb, (c) PAN-G@Sb at 1.0 mA/cm^2 with Na plating capacity of 2.0 mAh/cm^2, and the corresponding electrodes after Na stripping at 1.0 mA/cm^2 with 2.0 mAh/cm^2: (e) Cu, (f) G@Sb, (g) PAN-G@Sb. SEM image of PAN-G@Sb (d) plating and (h) stripping at 1.0 mA/cm^2 with 6.0 mAh/cm^2. (i-m) SEM image and the corresponding EDS elements mapping of cross-section of PAN-G@Sb in Na plating state at 1.0 mA/cm^2 with 2.0 mAh/cm^2.

which can only operate 13 cycles. The results of electrochemical impedance spectroscopy impedance analysis indicate PAN-G@Sb-Na anode show the lower charge transfer resistance and interfacial resistance than Cu-Na anode, suggesting its excellent reaction kinetics and stable interface (Fig. S12 and Table S1 in Supporting information). When the cell with a normal N/P ratio (15.2, loading mass of NVP reduced to 2.1 mg/cm^2), the Na-PAN-G@Sb||NVP has an energy density of 145.5 Wh/kg at a rate of 1 C (Fig. 4c), and achieves over 1600 cycles with a capacity retention of 96.03% (per cycle capacity decay rate of 0.0025%). The charge/discharge curves at different cycles also show its highly reversible Na storage performance (Fig. S13 in Supporting information). Benefiting from the synergistic effect of top 3D PAN protective layer and bottom G@Sb sodiophilic layer, the full cells demonstrate high energy density, long cycling life and superior capacity retention, which are rarely achieved in previous reported SMBs (Fig. 4d and Table S2 in Supporting information) [37-43]. The initial three cycles of cyclic voltammetry curves show that the Na-PAN-G@Sb||NVP cell displays smaller electrochemical polarization during charge and discharge than that of Na-Cu||NVP cells (Fig. S14 in Supporting information). Furthermore, the rate performance of Na-PAN-G@Sb||NVP cell at different current densities was tested (Fig. S15 in Supporting information), which obtain a discharge capacity of 108.5, 105.7 and 98.7 mAh/g at 2, 5 and 10 C rate.

Moreover, the anode-free full cell was also assembled using PAN-G@Sb substrate and high-loading NVP cathode ($\approx$ 7.7 mg/cm^2) to further investigate the practical feasibility of PAN-G@Sb. There is no active Na metal pre-deposited on the substrate. As shown in Fig. S16 (Supporting information), the cell (N/P ratio = 0) delivers a reversible capacity of 84.1 mAh/g with an initial CE of 72.5%, which increases to 99.4% after 6 cycles (Fig. 4e). The large irreversible capacity loss in the first cycle should be due to the formation of abundant SEI. The PAN-G@Sb||NVP cell exhibits a high energy density of 277.5 Wh/kg with excellent capacity retention of 91.0% after 50 cycles at 0.5 C (Fig. 4f), further confirming the key role of dual-layer host in the stable SMBs [19,44]. The results also indicate that PAN-G@Sb can be a potential candidate as promising current collector for high energy and high stable SMBs.

In summary, we have developed a 3D dual-layer host with sodiophilic G@Sb bottom layer and 3D PAN framework top layer by combining facile coating and electrospinning process. The dual-layer host can not only provide sufficient nucleation sites to induce homogeneous Na plating, but also regulate the stable and lateral Na growth. Therefore, the dual layer host exhibits an impressive Na plating/stripping for 1000 cycles at 2.0 mA/cm^2, and stable cycling in symmetric cells over 1000 h. The full cell with N/P ratio of 1.4 using NVP cathode and Na-PAN-G@Sb host displays a high energy density of 284.6 Wh/kg and excellent cycling stability with capacity retention of 98.7% after 250 cycles. Furthermore, after 50 cycles at 0.5 C, the PAN-G@Sb||NVP anode-free full cell also exhibits a superior capacity retention of 91.0%, illustrating the stable operation of high energy SMBs. This work provides a fresh insight into facile constructing high stability, high-performance and low costs 3D dual layer host for safe and high energy density SMBs.

Declaration of competing interests

The authors declare that they have no known competing financial interests or personal relationships that could have appeared to influence the work reported in this paper.

CRediT authorship contribution statement

Run Chai: Data curation, Methodology, Writing – original draft, Writing – review & editing. **Qiujie Wu:** Methodology. **Yongchao Liu:** Data curation. **Xiaohui Song:** Supervision. **Xuyong Feng:** Supervision. **Yi Sun:** Conceptualization, Supervision, Writing – original draft, Writing – review & editing. **Hongfa Xiang:** Project administration, Supervision.

Acknowledgments

This work was financially supported by National Natural Science Foundation of China (Nos. 52072105 and 21676067), the Key R&D Program of Anhui Province (Nos. 2023t07020007, 202104a05020044), the Major Science and Technology Projects in Anhui Province (Nos. 202203a07020027, 2021e03020001 and 2023z020003), Fundamental Research Funds for the Central Universities (Nos. PA2022GDGP0029, PA2023GDGP0042).

Supplementary materials

Supplementary material associated with this article can be found, in the online version, at doi:10.1016/j.cclet.2024.110007.

References

[1] J.B. Goodenough, K.S. Park, J. Am. Chem. Soc. 135 (2013) 1167–1176.
[2] D. Lin, Y. Liu, Y. Cui, Nat. Nanotechnol. 12 (2017) 194–206.
[3] H.S. Hirsh, Y. Li, D.H.S. Tan, et al., Adv. Energy Mater. 10 (2020) 2001274.
[4] M. Su, Y. Chen, S. Wang, et al., Chin. Chem. Lett. 34 (2023) 107553.
[5] X. Jin, Y. Li, S. Zhang, J. Zhang, et al., Chin. Chem. Lett. 33 (2022) 491–496.
[6] B. Lee, E. Paek, D. Mitlin, S.W. Lee, Chem. Rev. 119 (2019) 5416–5460.
[7] S.J. Yang, J.K. Hu, F.N. Jiang, et al., eTransportation 18 (2023) 100279.
[8] H. Wang, D. Yu, C. Kuang, et al., Chem 5 (2019) 313–338.
[9] H. Wang, E. Matios, J. Luo, W. Li, Chem. Soc. Rev. 49 (2020) 3783–3805.
[10] W. Liu, Y. Xia, W. Wang, et al., Adv. Energy Mater. 9 (2019) 1970007.
[11] Y. Wang, Y. Wang, Y.X. Wang, et al., Chem 5 (2019) 2547–2570.
[12] H. Wang, C. Wang, E. Matios, W. Li, Angew. Chem. 130 (2018) 7860–7863.
[13] J. Ma, X. Feng, Y. Wu, et al., J. Energy Chem. 77 (2023) 290–299.
[14] Q. Zhong, B. Liu, B. Yang, et al., Chin. Chem. Lett. 32 (2021) 3496–3500.
[15] M. Zhu, G. Wang, X. Liu, et al., Angew. Chem. 132 (2020) 6658–6662.
[16] S. Zhang, B. Cheng, Y Fang, et al., Chin. Chem. Lett. 33 (2022) 3951–3954.
[17] X.B. Cheng, S.J. Yang, Z. Liu, et al., Adv. Mater. 36 (2024) 2307370.
[18] H Gao, S Xin, L Xue, J.B Goodenough, Chem 4 (2018) 833–844.
[19] L. Lin, L. Suo, Y.S. Hu, et al., Adv. Energy Mater. 11 (2021) 2003709.
[20] L. Ye, M. Liao, T. Zhao, et al., Angew. Chem. 131 (2019) 17210–17216.
[21] Y. Xu, C. Wang, E. Matios, et al., Adv. Energy Mater. 10 (2020) 2002308.
[22] X. Chen, Y.K. Bai, X. Shen, et al., J. Energy Chem. 51 (2020) 1–6.
[23] S. Tang, Z. Qiu, X.Y. Wang, et al., Nano Energy 48 (2018) 101–106.
[24] R. Zhuang, X. Zhang, C. Qu, et al., Sci. Adv. 9 (2023) eadh8060.
[25] Y. Liu, Y. Zhen, T. Li, et al., Small 16 (2020) 2004770.
[26] G. Wang, Y. Zhang, B. Guo, et al., Nano Lett. 20 (2020) 4464–4471.
[27] K.B. Hatzell, ACS Energy Lett. 11 (2023) 4775–4776.
[28] J. Lee, S.H. Jeong, J.S. Nam, et al., EcoMat (2023) e12416.
[29] W. Liu, Z. Chen, Z. Zhang, et al., Energy Environ. Sci. 14 (2021) 16472.
[30] P. Albertus, S. Babinec, S. Litzelman, A. Newman, Nature Energy 3 (2018) 16–21.
[31] W. Liu, P. Liu, D. Mitlin, Adv. Energy Mater. 10 (2020) 2002297.
[32] W. Liu, Y. Luo, Y. Hu, et al., Adv. Energy Mater. 14 (2024) 2302261.
[33] K. Lee, Y.J. Lee, M.J. Lee, et al., Adv. Mater. 34 (2022) 2109767.
[34] B. Sun, P. Li, J. Zhang, et al., Adv. Mater. 30 (2018) 1801334.
[35] S Tas, O Kaynan, E Ozden-Yenigun, K Nijmeijer, RSC Adv. 6 (2016) 3608–3616.
[36] B.D. Adams, J. Zheng, X. Ren, et al., Adv. Energy Mater. 8 (2018) 1702097.
[37] Z. Sun, Y. Ye, J. Zhu, et al., Small 18 (2022) 2107199.
[38] Z. Zhang, L. Li, Z. Zhu, et al., Energy Storage Mater. 53 (2022) 363–370.
[39] J. Zhang, S. Wang, W. Wang, B. Li, J. Energy Chem. 66 (2022) 133–139.
[40] Y. Liu, X. Liu, G. Zhang, et al., ACS Appl. Mater. Interfaces 15 (2023) 26691–26699.
[41] B. Liu, D. Lei, J. Wang, et al., Nano Res. 13 (2020) 2136–2142.
[42] Z. Li, H. Qin, W. Tian, et al., Adv. Funct. Mater. 29 (2024) 2301554.
[43] L. Zhao, Z. Hu, Z. Huang, et al., Adv. Energy Mater. 12 (2022) 2200990.
[44] S. Wu, J. Hwang, K. Matsumoto, R. Hagiwara, Adv. Energy Mater. 13 (2023) 2302468.